Physicochemical Characterization of Biomaterials Commonly Used in Dentistry as Bone Substitutes—Comparison with Human Bone

Margarida Figueiredo,[1] Jose Henriques,[2] Gabriela Martins,[1] Fernando Guerra,[2] Fernando Judas,[3] Helena Figueiredo[4]

[1] Chemical Engineering Department, University of Coimbra, 3030-290 Coimbra, Portugal

[2] Department of Dentistry, University of Coimbra, 3030-005 Coimbra, Portugal

[3] Orthopaedics Department, Coimbra University Hospital, Hospitais da Universidade de Coimbra, 3000-075 Coimbra, Portugal

[4] Histology Institute, University of Coimbra, 3004-504 Coimbra, Portugal

Received 27 October 2008; revised 30 May 2009; accepted 27 July 2009
Published online 10 November 2009 in Wiley InterScience (www.interscience.wiley.com). DOI: 10.1002/jbm.b.31529

Abstract: The present work focuses on the physicochemical characterization of selected mineral-based biomaterials that are frequently used in dental applications. The selected materials are commercially available as granules from different biological origins: bovine, porcine, and coralline. Natural and calcined human bone were used for comparison purposes. Besides a classical rationalization of chemical composition and crystallinity, a major emphasis was placed on the measurement of various morphostructural properties such as particle size, porosity, density, and specific surface area. Such properties are crucial to acquiring a full interpretation of the *in vivo* performance. The studied samples exhibited distinct particle sizes (between 200 and 1000 μm) and shapes. Mercury intrusion revealed not only that the total sample porosity varied considerably (33% for OsteoBiol®, 50% for PepGen P-15®, and 60% for BioOss®) but also that a significant percentage of that porosity corresponded to submicron pores. Biocoral® was not analyzed by this technique as it possesses larger pores than those of the porosimeter upper limit. The density values determined for the calcined samples were close to the theoretical values of hydroxyapatite. However, the values for the collagenated samples were lower, in accordance with their lower mineral content. The specific surface areas ranged from less than 1 m^2/g (Biocoral) up to 60 m^2/g (BioOss). The chemical and phase composition of most of the samples, the exception being Biocoral (aragonite), were hydroxyapatite based. Nonetheless, the samples exhibited different organic material content as a consequence of the distinct heat treatments that each had received. © 2009 Wiley Periodicals, Inc. J Biomed Mater Res Part B: Appl Biomater 92B: 409–419, 2010

Keywords: bone graft; FTIR; hydroxy(1)apatite; morphology; porosity

INTRODUCTION

Bone grafts are frequently used in orthopedics, periodontics, and in oral and maxillofacial surgery with effective clinical outcomes.[1–9] This approach has been used routinely as a treatment for bone regeneration in osseous defects.

Although the greatest success in bone grafting has been achieved with autogeneous bones, such use is constrained by limited material supply and donor site morbidity.[1,5,6] Numerous biomaterials have been successfully used as bone substitutes, such as allografts, xenografts, natural and synthetic calcium-based materials, and a combination of these.[5,7,9] Allografts do not have the drawbacks of autografts but are less successful in clinical practice. They also carry several other disadvantages. These include the risk of disease transmission or infection, difficulties in obtaining and processing, and rapid resorption.[1–7] Also, mechanical strength is partially lost after sterilization.[4,9,10] Allogeneic bone is usually processed as a freeze-dried graft or as a demineralized bone matrix (DBM). The former, while osteoconductive, has no osteogenic or osteoinductive capabilities, being usually placed in conjunction with autogenous grafts.[1,5,6] DBM, on the other hand, retains some osteoinductive properties as a consequence of the demineralization

Correspondence to: M. Figueiredo (e-mail: mmf@eq.uc.pt)

process that may expose native matrix proteins, such as bone morphogenetic proteins (BMPs).[11,12]

Xenografts have been regarded as promising alternatives to autografts, given that xenografts represent an unlimited supply of available material and may reduce morbidity by eliminating the donor site. Xenogeneic bone, mainly of bovin origin, was popular in the 1960s but fell into disfavor because of immunogenicity risks. The reintroduction of these products, more recently, came after the development of safer methods to deproteinate bone particles, namely by heat treatment.[13,14] Although most of the xenografts that are currently used have porcine and bovine origins, because of their similarity to the human bone regarding chemical composition (mainly carbonated hydroxyapatite and type I collagen) and structure,[1,5,7,9] the interest in natural coral exoskeletons has been increasing. This is because natural coral exoskeletons give reduced risk of disease transmission and viral contamination compared with the risks posed by bovine grafts.[1,2,5,7,9,15] Coral is composed of calcium carbonate in the form of aragonite. It has achieved considerable success in bone-graft applications because of its large porosity and uniform pore size (which can range from 100 to 500 μm) combined with mechanical strength. Although there are hundreds of genera of coral, only a few meet the required standards of pore diameter and connectivity.[2,7,9,15] Nonetheless, unconverted coral is unsuited for most long-term implants because of its high dissolution rate, poor longevity, and poor stability.[9,16] High degradation rates have also been found at low pH values (5.0–6.5), which are normally associated with infections and inflamed tissues. To overcome this limitation, corals have been converted into hydroxyapatite (coralline hydroxyapatite) by hydrothermal exchange or microwave processing, leading to products with improved resorption rates and better osteointegration.[9,16,17] In this treatment, hydroxyapatite partially replaces aragonite while preserving the porous structure. However, under certain circumstances, a decrease in structural strength may be observed.[17] This problem can be reduced through the use of double-conversion techniques (conversion to coralline apatite followed by sol–gel nanocoating).[9]

To avoid the main shortcomings of allografts and xenografts, products of synthetic origin are increasingly being developed with the objective of fabricating biomaterials that mimic the extracellular matrix of bone with not only respect to the chemical composition but also to structural and functional properties.[18–20] In the recent past, many calcium phosphate-based materials have been employed in the fabrication of porous scaffolds, whose Ca/P ratios have been varied to produce compounds ranging from calcium tetraphosphate (Ca/P = 2), hydroxyapatite (Ca/P = 1.67), tricalcium phosphate (Ca/P = 1.5), to anhydrous dicalcium phosphate (Ca/P = 1).[21–23] For similar structures, those with a low Ca/P ratio resorb more rapidly, giving rise to unpredictable biodegradation profiles and resulting in undesirable loss of mechanical strength.[21–25] On the contrary, those with greater Ca/P ratios degrade more slowly but may give rise to remnants that can induce inflammation. In addition, lower degradation rates usually result in less new bone formation around the scaffold. The combination of different calcium phosphates products can be used as a strategy to control resorption rates.[22–24]

However, the chemical composition alone is by no means the only factor in determining the nature and extent of scaffold biodegradation. Besides physiological conditions, characteristics such as crystallinity, crystal size, particle size and size distribution, porosity and surface roughness have been reported to influence the biological performance.[24–27]

Finally, introducing osteoactive agents in scaffolds, by loading or by promoting chemical bonding, has been adopted as a method for stimulating the deposition of bone. These agents include bone BMPs, cells (osteoblasts, bone marrow cells),[20,28,29] and other bioactive molecules (for example, P-15 aminoacid sequence).[8,30,31]

Nevertheless, despite all efforts regarding the development of biomaterials to be used as bone grafts, no available biomaterial is as good as autografts in overall performance.[1–6]

The main purpose of this study was the characterization of a variety of granulate mineral-based biomaterials, which are both commercially available and frequently used for dental applications as bone substitutes. These materials were chosen to encompass materials of different origins (bovine, porcine, and coralline) and different types (cortical and cancellous bone and mineral based), including biomimetic factors, covering a wide range of products/applications. Some of these graft materials have been thoroughly characterized for their physico/chemical properties, using techniques such as high resolution X-ray diffractometry (XRD), infrared spectroscopy, and thermogravimetry.[32] However, characteristics such as the shape and size (for those materials that are in a granular form) and morphostructural features, which play an important role on the materials' *in vivo* performance, have not been fully explored. Beside the chemical composition, it is known that surface area and topography (mainly pore size) exert a major influence over the interaction of osteogenic cells with the biomaterial surface.[27,33] The particle size, for instance, affects not only the contact area but also the packing characteristics of the materials, ultimately determining the macroporosity of the particle ensemble (crucial for bone regeneration).[26,34] Additionally, recent studies have demonstrated that microporosity can also be used to accelerate osseointegration.[27,35,36]

The emphasis of this work concerned the determination of the physical characteristics, specifically particle size, porosity, density, and surface area. These parameters were evaluated using laser spectrometry, image analysis, mercury porosimetry, gas pycnometry, and gas adsorption. Comparison with the data supplied by manufacturers is provided when available. Sample characterization was complemented by Fourier transform infrared spectroscopy (FTIR) and XRD analysis. Comparisons of the properties of the com-

mercial products with the properties of human bone were also fully explored. Moreover, as some of the tested materials were anorganic in type and processed using different thermal treatments, this study also covers both natural and calcined human bones.

MATERIALS AND METHODS

The biomaterials examined included grafting materials of different origins: bovine (BioOss® and PepGen P-15®), porcine (OsteoBiol®), and coralline (Biocoral®). These samples were characterized as supplied (i.e., with no further treatment). BioOss is derived from cancellous bone, PepGen P-15 from cortical bone, and OsteoBiol is constituted as a mixture of these two types of bone (80% cancellous and 20% cortical). In addition, PepGen P-15 contains biomimetic factors (P-15 aminoacid sequence).

Each material was used in a granular form (easier to accommodate and more quickly resorbed) with the lowest particle size range available, recommended for application in the treatment of oral, periodontal, and maxillofacial bone defects.

BioOss spongiosa granules, produced by Geistlich Pharma AG (Wolhusen, Switzerland), are reported to be a natural bone mineral, derived from bovine bone and containing carbonate apatite. The granules are deorganified by means of a proprietary extraction process (treatment with strong alkalis and organic solvents, up to 300°C) that allegedly renders the substrate antigenic and protein free.[37] This material was used as granules of 250–1000 μm.

PepGen P-15 (Dentsply Friadent, Mannheim, Germany), available as a granulate (250–420 μm), is also an anorganic bovine material that is composed of pure polycrystalline hydroxyapatite, created as a result of thermal processing at 1100°C, completely removing proteins from bone. After calcination, a sequence of 15 amino acids of Type I collagen were added to the mineral component.[38]

OsteoBiol (Tecnoss Dental, Pianezza, Italy), used as 250–1000 μm granules, is a xenograft material of porcine origin, processed at low temperature (maximum of 130°C) to completely eliminate any pathogenic elements. The preservation of the structure and composition of the natural collagen and hydroxyapatite was maintained.[39]

Biocoral (Inoteb, St. Gonnery, France), a coralline derived sample, is claimed to be a highly pure (>98%), bioresorbable, calcium carbonate material in the form of aragonite, with pore sizes up to 500 μm. According to the producers, Biocoral presents good hemostatic properties that are not altered by processing.[40] The particle size range selected for this study was 630–1000 μm (ref MIG 1-1).

As mentioned earlier, the results obtained for these biomaterials were compared with those of human bone. Thus, a human cortical bone (gamma-irradiated and freeze-dried femoral diaphysis, from a male, 39-year-old donor), provided by the bone bank of Coimbra University Hospital (HUC Bone and Tissue Bank, Coimbra, Portugal[41]), was subsequently segmented and, as described later, subjected to the same characterization as the commercial samples.

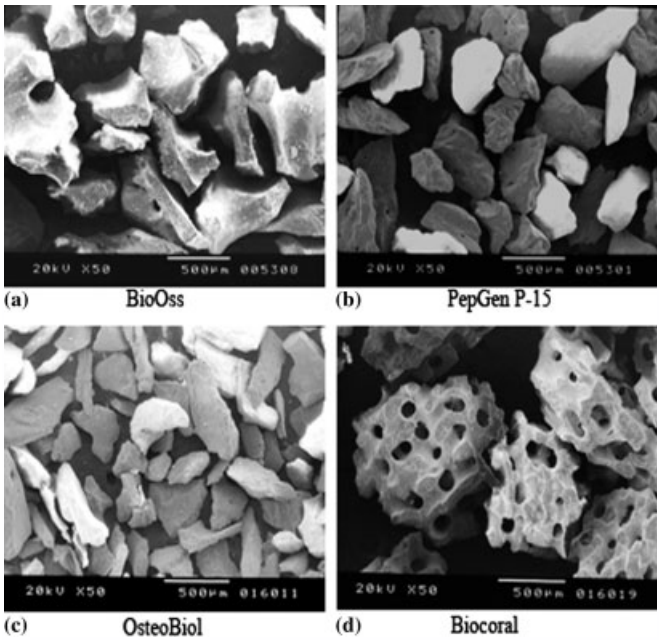

Figure 1. Morphology of the commercial granular samples: (a) BioOss, (b) PepGen P-15, (c) OsteoBiol, and (d) Biocoral. The SEM images show different shapes and structural features for various particulate materials.

The diaphysis was cross-sectioned into similar segments (1.5 cm thickness) that were degreased through immersion in an alcohol series (ethanol at 70% v/v), followed by washing with distilled water. Afterward, samples were kept in 30% v/v hydrogen peroxide for 48 h and rinsed again. The cleaned segments were stored in formaldehyde solution (4% v/v) at 4°C. Before use, the segments were thoroughly rinsed with distilled water and dried at 50°C for 3 days, being herein designated as "natural bone."

To prepare samples that could be compared to the commercial anorganic samples, some of these segments were calcined at 600°C in a muffle furnace under normal atmosphere, with a heating ramp rate of 10°C/min from room temperature. Samples were maintained at 600°C and were periodically weighed to constant weight. Then, they were naturally cooled and kept in a desiccator.

Analytical-grade hydroxyapatite and collagen samples (purchased from Sigma-Aldrich, Germany) were also used, namely in the FTIR analysis, to compare their spectra with those of the bone samples.

Figure 1 illustrates the morphological aspect of the commercial samples that were tested in granular form. Images were obtained by scanning electron microscopy (SEM), using a JSM-530 (Jeol Ltd, Tokyo, Japan) microscope operating at 20 kV. The samples were mounted on double-coated, carbon-conductive tape and then sputter-coated with gold.

These materials were first characterized for their particle size. Laser diffraction spectrometry (Coulter LS 130, Beck-

man Coulter Inc., Fullerton, CA) was used.[42] Three independent measurements were performed for each sample. The equipment software automatically computes the average particle size distribution and the corresponding statistical parameters, with 0.95 confidence level.

Most of the samples contained particles that were larger than the upper limit of the equipment (900 μm). Hence, these samples were further analyzed by image analysis with BH-2 microscope (Olympus) coupled with morphometry software CUE-2 also from Olympus (Olympus Corp., Lake Success, NY). The number of counted particles was selected in such a way that a deviation of 5% relative to the arithmetic average diameter (at a 95% confidence level) was reached. This counting corresponded to at least 500 particles.

Information concerning the sample porosity and the pore size distribution was obtained by mercury intrusion[43,44] using the Poresizer 9320 (Micromeritics Instrument Corp., Norcross, GA) in a pressure range between 0.05 and 2000 atm, corresponding to a range of pore diameters between 400 μm and 0.006 μm, respectively. From the pressure versus intrusion data, the equipment generates pore size distributions, using the Washburn equation [Eq. (1)].

$$d = \frac{4\gamma \cos\theta}{P} \tag{1}$$

Based on the cylindrical pore geometry, this expression relates the pore diameter (d) with the mercury surface tension (γ), the contact angle between mercury and the solid surface (θ), and the applied pressure (P) necessary for mercury to penetrate the sample pores. In the present work, γ was taken as 0.48 N m^{-1} and θ as 140°.

The porosity was calculated as the ratio of the intruded volume and the total sample volume, including all open voids, as expressed by Eq. (2).

$$\text{Porosity} = \frac{V_{\text{Empty Spaces}}}{V_{\text{Solid Material}} + V_{\text{Empty Spaces}}} \tag{2}$$

Two samples (~2.5 g) were analyzed by this technique. A third sample was additionally used if the measured porosity values differed by more than 5%. One of the samples was chosen to illustrate the pore size distribution, presented in the "Results" section. It should be noted that this technique uses a relatively large amount of material (thus ensuring sample representativeness) that cannot be further used (as it will be mercury contaminated).

The particles' real density (sample mass/volume of the solid (excluding empty spaces)) was determined by gas pycnometry[44] (Accupyc 1330 from Micromeritics Instrument Corp.). This measuring method excludes sample interstices and most pores, since the small volume of the gas molecules (He) enables their penetration in almost all empty spaces. An exception is given by the sample's closed pores, that is, those pores that are not opened to the surface. The density, measured in this way, provides the closest value to the solid density of the sample, justifying the use of the term "real" or "true" density.

At least 10 runs were performed for each sample, and at least three different samples were analyzed for each material. The coefficient of variance was used to compare mean values, with 5% as significance level.

The specific surface area of the samples were measured by the nitrogen adsorption technique (ASAP 2000 from Micromeritics Instrument Corp.), based on BET theory.[43,44] The samples analyzed by this method were the same as those subjected to porosimetry. As mentioned, at least two independent samples were measured for each material using the same validation criteria.

FTIR was used to provide information concerning the chemical composition and the major functional groups. Spectra were recorded in the range 500–4000 cm^{-1} in increments of 1.928 cm^{-1}, using a Magna FR-750 spectrometer (Nicolet,Madison, WI), in the attenuated total reflection (ATR) mode. Each spectrum was collected at room temperature at a resolution of 4 cm^{-1}, and the number of sample scans was 32.

XRD was used to identify phase and composition features and qualitatively evaluate the crystallinity of the materials. Diffraction data were collected using an X-PERT diffractometer, (Philips, Amsterdam, Netherlands), operating in the Bragg-Brentano configuration with Co-Kα radiation (λ =1.78897 Å) at a current of 35 mA and an accelerating voltage of 40 kV. Spectra were recorded in the range $10° < 2\theta < 70°$ at a scanning speed of 0.5°/min and step size of 0.02°. The obtained X-ray patterns of samples were compared with the patterns given by hydroxyapatite and aragonite and the corresponding data from International Centre for Diffraction Data (ICDD; Powder Diffraction Files n° 84-1998 and 75-2230).

RESULTS

Particle Size Analysis

Table I contains the particle size parameters (in volume percentages) of the commercial samples in terms of median diameter (D_{50}), as well as the particle size range, expressed by the 10% and 90% percentiles (D_{10} and D_{90}) and in nondimensional form ($(D_{90} - D_{10})/D_{50}$). Also in Table I are the size ranges reported by the manufacturers.

The first conclusion to be drawn from these results is that PepGen P-15 has the lowest particle size (approximately half of the other samples), confirming the observations of Figure 1. Second, PepGen P-15 and OsteoBiol correspond to the broader size distributions. In contrast, Biocoral presents the most homogeneous size distribution. The experimentally determined size ranges, although not

TABLE I. Particle Size Parameters (in Volume Percentages) of the Commercial Samples

Sample	Median Size[a] (D_{50}, μm)	Size Range[a] ($D_{10}-D_{90}$,μm)	Size Range (Nondimensional) $(D_{90}-D_{10})/D_{50}$	Size Range Reported by Producers (μm)
Bio-Oss[b]	740	510–1030	0.7	250–1000
PepGen P-15[c]	367	180–558	1.02	250–420
OsteoBiol[b]	810	455–1260	0.99	250–1000
Biocoral[b]	980	765–1010	0.25	640–1000

Median diameter (D_{50}), size range expressed in percentiles (D_{10} and D_{90}) and in nondimensional form [$(D_{90} - D_{10})/D_{50}$]. The size range reported by the producers is also presented for comparison. These values show that the PepGen P-15 particles are the smallest in size and that the Biocoral particles have the narrowest size distribution. The size ranges are relatively close to those reported by the producers.

[a] D_{10}, D_{50}, and D_{90}: particle diameters corresponding respectively to 10, 50, and 90 % of the cumulative size distribution curve.

[b] Image analysis.

[c] Laser diffraction.

coincident with the information supplied by the producers[37–40] are, nevertheless, relatively close.

Mercury Intrusion

When analyzing a granular material by mercury porosimetry, two kinds of voids can be detected: those that correspond to the empty spaces between the particles (commonly designated by "interstices" or "interparticle" spaces) and those that correspond to the voids of the particles themselves (known as "pores" or "intraparticle" spaces). The results obtained for the granules of BioOss (Figure 2) show that with increasing pressure, mercury penetrates to the increasingly smaller pores. The cumulative curve [Figure 2(a)] denotes a small intrusion in pores between 400 μm (upper limit detection) and 10 μm, followed by a plateau between 10 and 0.2 μm where no intrusion is detected, and then a significant mercury penetration into pores that are smaller than this value. The initial rise of the curve corresponds mostly to the filling of the voids between the particles (and may also include some of the largest pores of cancellous bone), whereas the later stage of rise is related to the pores of the individual particles. The range of the intraparticle pores is more obvious in Figure 2(b), in which one intense peak whose mode is about 0.03 μm is clearly visible. The smaller peak on the left (>100 μm) corresponds to the intrusion of the mercury in the interparticle voids. The size of these voids, related to the way the particles are packed, depends on the particle size and shape as well as the particle size distribution. However, the distinction between inter- and intraparticle voids is not always so apparent. This interpretation aims to elucidate the kind of information that can be extracted from the pore size distribution curves and highlight the importance of always specifying the size range of the measured pores. It should be stressed that the mercury intrusion technique is especially suited to the analysis of intraparticle pores, being not so adequate to the measurement of large voids (>400 μm). Because of this limitation, this technique was not used with the Biocoral granules, since these possess a large proportion of very big pores, not completely measurable, thus leading to a significantly underestimated porosity value.

The intrusion curves (cumulative intruded volume versus pore diameter) of the three samples that were analyzed in their granular form are depicted in Figure 3(a). Figure 3(b) presents the corresponding differential pore size distributions. Table II summarizes these results in terms of the total intruded volume, mode of intraparticle pores, total porosity, and intraparticle porosity (taken as the percentage of the particles internal pores (<1 μm), relative to the total porosity). Analysis of Table II and Figures 4 and 5 suggests that BioOss has the greatest porosity, being the measured value in agreement with that reported by the producer (60%, also obtained by mercury intrusion[37]). However, about half of this porosity corresponds to submicron pore entrances. Smaller porosity values were determined for the PepGen P-15 and OsteoBiol samples. These also exhibit a much smaller proportion of submicron pores. An interesting feature detected for PepGen P-15 is that the mode found for the intraparticle pores (0.3 μm) is about 10 times larger than that of the other two samples.

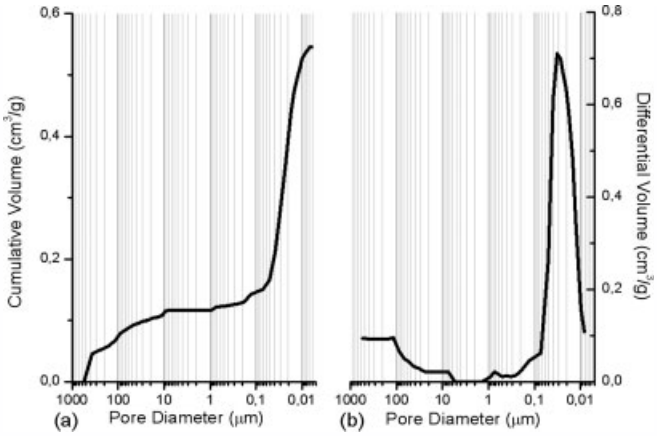

Figure 2. Mercury intrusion curves of BioOss measured by mercury porosimetry: cumulative intruded volume versus pore diameter (a) and differential-intruded volume versus pore diameter (b). The intrusion profiles show a small mercury penetration into pores between 400 and 10 μm (interparticle pores) and a significant mercury penetration into pores smaller than 0.2 μm (intraparticle pores).

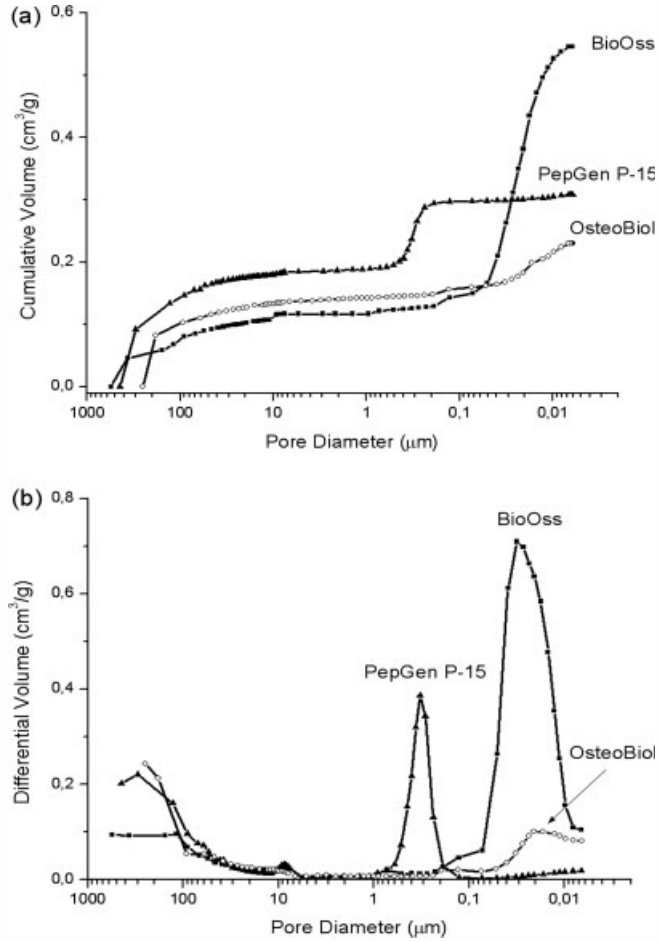

Figure 3. Cumulative (a) and differential (b) intrusion curves of BioOss, PepGen P-15, and OsteoBiol measured by mercury porosimetry. BioOss presents the highest intrusion volume whereas OsteoBiol gives the lowest. Differential curves show that BioOss exhibits intraparticle pores around 0.03 μm, similar to those of OsteoBiol but 10 times less than those of PepGen P-15.

Table III gives the total intruded volume and porosity that was measured for the human cortical bone before and after calcination. The natural human cortical bone (noncalcined) presents a low porosity value, as expected, since it is a compact bone. Subjecting the cortical bone to calcination at 600°C resulted in an increase in the porosity from

TABLE II. Mercury-Intruded Volume, Mode (Most Frequent Diameter) of Intraparticle Pores, Total Porosity, and Intraparticle Porosity of the Commercial Samples

Sample	Intruded Volume[a] (cm^3/g)	Mode of Intraparticle Pores (μm)	Total Porosity[a] (%)	Intraparticle Porosity[b] (%)
BioOss	0.546	0.03	63.5	51
PepGen P-15	0.308	0.3	49.4	23
OsteoBiol	0.230	0.02	33.1	21

BioOss exhibits the highest porosity. However, about half of this porosity is derived from submicron pores.

[a] Corresponding to pores <400 μm.

[b] Corresponding to pores <1 μm.

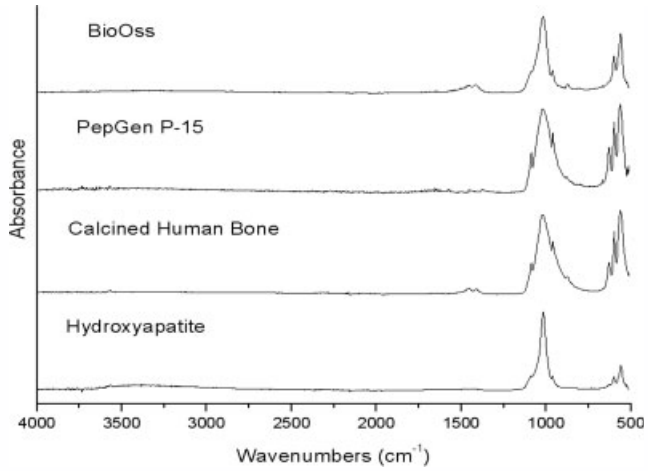

Figure 4. FTIR spectra of BioOss, PepGen P-15, calcined human bone, and hydroxyapatite (from top to bottom). All of the samples are mainly composed of hydroxyapatite. Additionally, BioOss and calcined human bone exhibit a small peak at around 1400 cm^{-1}, characteristic of the carbonate group.

6% to 33%. However, the consequence of this heat treatment was to increase not only the porosity but also the pore size. As mentioned earlier, the particles of PepGen P-15, thermally treated at high temperatures (1100°C), also possess intraparticle pores of the same size.

Density

The results from the gas pycnometry study, listed in Table IV, show that the higher densities were measured for BioOss and PepGen P-15. These values are quite close to the theoretical density of the hydroxyapatite crystal ($Ca_{10}(PO_4)_6(OH)_2$), reported to be 3.16 g/cm^3.[45] The value obtained for Biocoral coincides with the specific gravity of aragonite (2.93),[46] a mineral that is composed of calcium carbonate. These results support the measured values (and the suitability of the technique). They also give a guide to the purity of these samples. The lower values correspond, as expected, to the collagenated samples (OsteoBiol and natural human bone). The calcination of the natural bone resulted in an increase in density, bringing the value close to the theoretical value for hydroxyapatite. The density values are also consistent with the mineral content of each sample.

Surface Area

The specific surface area of each of the samples, in granular form, were determined by the gas adsorption technique (BET). The results are listed in Table V. These values depend on the type of sample (cortical or cancellous bone), being a consequence of their surface characteristics. The largest value was achieved for the granules of BioOss, closely followed by those of OsteoBiol. The remaining samples exhibit much lower values.

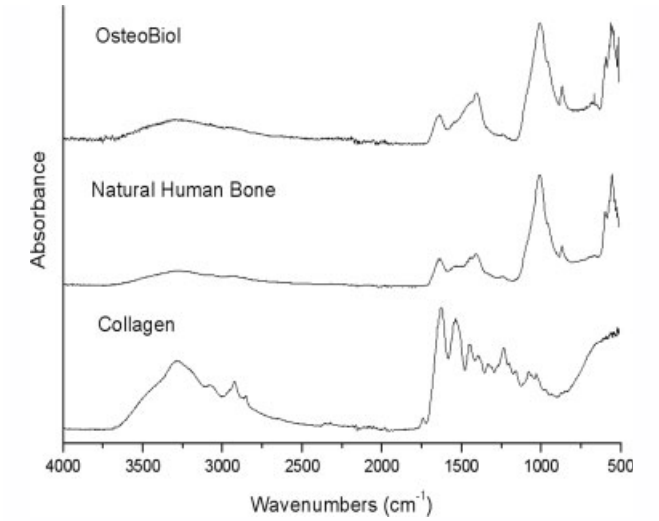

Figure 5. FTIR spectra of OsteoBiol, natural human bone, and collagen. As expected, collagen bands are clearly visible in addition to those of hydroxyapatite.

FTIR

The infrared spectra are given in Figures 4 and 5. Figure 4 includes the spectra of BioOss, PepGen P-15, and calcined human bone as well as the spectrum of hydroxyapatite, the main constituent of these samples. As expected, they all show the typical bands originated by this mineral. These are the more intense phosphate stretching bands observed at around 1010 cm^{-1} and 560 cm^{-1}.[32,47,48] Both the Bio-Oss granules and calcined human bone present, in addition, a low-intensity double band at 1410–1460 cm^{-1} that corresponds to stretching vibrations of CO_3^{2-}, substituting for phosphate in the apatite lattice. However, this CO_3^{2-} band is absent in the spectrum of PepGen P-15, certainly as a result of the high calcination temperature to which this sample was subjected (1100°C).[32,49] Human bone samples that were calcined at 600°C exhibited the carbonate band. However, the intensity was less than that seen for BioOss, indicating a lower CO_3^{2-} content. The organic content of PepGen P-15 was not detected in the FTIR spectrum, probably because of the small amount present (less than 1.2%).[32]

The second group of vibrational spectra, depicted in Figure 5, include the spectra relating to the collagenated samples, OsteoBiol and natural human bone spectra, together with the spectrum of Type I collagen for the sake of comparison. Although both samples have different origins (porcine and human), their spectra are very similar. As before, the mineral constituent (hydroxyapatite) gives the most intense peak at 1010 cm^{-1}, as well as the bands occurring at lower wavenumbers. Above 1300 cm^{-1}, almost all of the bands are exclusively assigned to collagen vibrations, the exception being those originated by CO_3^{-2} at 1410 and 1460 cm^{-1}.[32,47]

The FTIR spectrum of Biocoral was compared with that of calcium carbonate. Both spectra were coincident, indicating that Biocoral is composed of pure $CaCO_3$.

TABLE III. Mercury-Intruded Volume, Mode of Intraparticle Pores, and Total Porosity of the Human Cortical Bone Before and After Calcination

Sample	Intruded Volume (cm^3/g)	Mode of Intraparticle Pores (μm)	Total Porosity (%)
Natural human bone	0.032	0.02	6.2
Calcined human bone	0.221	0.25	33.1

Heat treatment at 600°C gives rise to a sixfold increase in the porosity and a tenfold increase in the intraparticle pore size.

TABLE IV. Real Density (ρ), as Measured by Helium Pycnometry, and Mineral Content (Derived from Calcination at 600°C) of the Different Commercial Biomaterials and of Human Bone (Before and After Calcination)

	Sample	ρ[a] ($g\ cm^{-3}$)	Mineral Content[a] (wt %)
Xenograft	Bio-Oss	3.21	95.0
	PepGen P-15	3.20	98.8
	OsteoBiol	2.43	64.6
	Biocoral	2.92	96.4
Allograft	Natural human bone	2.30	65.0
	Calcined human bone	3.10	100.0

The density of anorganic samples is practically coincident to that of hydroxyapatite (3.16). The density of the collagenated samples is consistent with their mineral content (~65%).

[a] Mean value (CV < 0.05).

XRD

The XRD results can be associated with the chemical composition of the respective samples (Figure 6). Thus, diffractograms from BioOss, PepGen P-15, and calcined human bone (mineral samples) are compared with the spectrum of hydroxyapatite [Figure 6(a)]. The spectra of the collagenated samples (OsteoBiol and natural human bone) are grouped in Figure 6(b).

As expected, the XRD pattern from the mineral samples correspond to hydroxyapatite,[48–50] with coincident peak positions and relative intensities. However, these materials present diverse degrees of crystallinity, as indicated in the

TABLE V. Specific Surface Area of the Samples in Granular Form Determined by Gas Adsorption (BET)

Sample	Specific Surface Area ($m^2\ g^{-1}$)
Bio-Oss	59.7
Pep-Gen P15	1.72
OsteoBiol	42.4
Biocoral	0.26

The measured values reflect the origin of the samples: BioOss (100% cancellous bone) exhibits the highest value; Osteobiol possesses a lower surface area (~80% of BioOss, in agreement with its composition (80% of cancellous bone)). The value for PepGen P-15 corresponds to the lowest value of the bone-derived samples, as a consequence of its cortical nature and also of alterations induced by the high-temperature treatment.

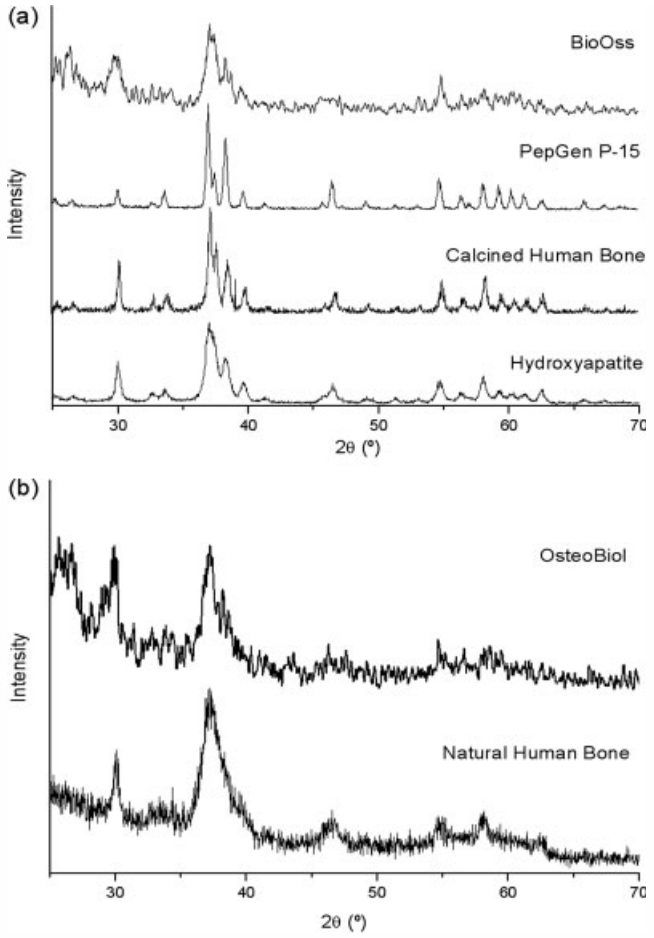

Figure 6. Diffractograms of BioOss, PepGen P-15, calcined human bone, and hydroxyapatite (a) and of OsteoBiol and natural human bone (b). Samples of the first group (a) although solely constituted of hydroxyapatite exhibit different degrees of crystallinity (different peak widths); samples of the second group (b) represent the dual-phase composition [hydroxyapatite (sharp peaks) and collagen (broad band)].

different peak widths. That is the case of BioOss, whose diffractogram exhibits broad peaks with a low signal-to-noise ratio, corresponding to a low-crystallinity material. On the other hand, the sharp and well-resolved peaks found in the XRD spectrum of PepGen P-15 indicate a highly crystalline hydroxyapatite. This is to be expected since this sample was subjected to high-temperature calcination (1100°C). Human bone that was calcined at a lower temperature (600°C) gives sharper diffraction peaks than those of BioOss and hydroxyapatite but broader than that of PepGen P-15.

The diffactograms of OsteoBiol and natural human bone [Figure 6(b)] represent the dual-phase composition of these samples. This is because each spectrum presents the more intense characteristic peaks of hydroxyapatite, superimposed on a broad band arising from collagen.

A similarity in the diffraction pattern of calcium carbonate (ICDD File n° 75-2230) and the XRD spectrum of Biocoral was observed (data not shown), confirming that this sample is composed of $CaCO_3$.

DISCUSSION

From the particle-size related data (Table I), it can be concluded that, in general, the size ranges measured for the materials tested, although different from those reported by the manufacturers, are similar. It should be noted that most producers do not specify the technique that was used in the characterization and that may be responsible for the differences observed.[51] SEM pictures have shown that the samples exhibit irregular and sharp-edge particles, whose sizes vary considerably (the median size ranges from about 350–1000 μm).

The likely influence of these properties and characteristics on the biological response cannot be easily predicted as the published studies involve different types of hydroxyapatite (natural and synthetic) in different particle size ranges. This observation applies to both *in vitro* and *in vivo* studies (the latter comprising distinct animal models).[34,52,53] For the ranges of particle size that were tested in this investigation, it has been reported that smaller particles (around 300 μm) are the basis of a better performance.[26,34,52,53] However, it should be kept in mind that the granules under analysis differed not only in their size but also in other physicochemical properties.

The measured porosity values (Table II) varied from 33% (OsteoBiol) to 63% (BioOss). The majority of the studies that are published in the literature present only total porosity values.[15,17,19,22] However, it is information concerning the pore size distribution that may be the more relevant to anticipating scaffold performance. A detailed analysis of the pore size distribution curves that were obtained by mercury intrusion revealed that, while the major contribution seems to derive from the 3D array of the particles (interparticle pores), an important part of porosity results from intraparticle pores (in some cases up to 50%, as found for BioOss). These pores present modes of 0.02 μm for BioOss and OsteoBiol and 0.3 μm for PepGen P-15.

With respect to the effect of porosity on bone regeneration, there is some controversy in the published literature. Although it is generally recognized that large pores (>100 μm) enhance new bone formation because they allow migration and proliferation of osteoblasts and mesenchymal cells,[54] it has also been reported that the presence of microporosity alters the pattern and dynamics of osteointegration[35,36] and might enhance ionic exchange with body fluids.[27] Moreover, it has been shown that nanoporous structure improve cell adhesion, proliferation, and differentiation.[34,55] Nevertheless, pore interconnectivity has been mentioned as a major benefit.[56] In the present case, as samples are in granular form, interconnectivity is naturally ensured. Even so, the differences detected, either in the total porosity or in the pore size can be expected to lead to distinctive *in vivo* behavior for the samples.

The comparison between natural and calcined human bone (Table III) has shown that the calcination process causes a significant increase in the total porosity as well as

the pore size. The calcined cortical bone is nearly five times more porous than the natural bone (6 vs. 33%), and the pore size increased tenfold (from 0.02 to 0.25 μm). Similar intraparticle pore sizes were detected for PepGen P-15 particles, which were also subjected to a high-temperature treatment (1100°C). This increase in porosity, induced by temperature, is due to the removal of the organic constituents that are associated with bone. Thus, heat treatment can be regarded as a convenient way to enhance the porosity of compact bones. However, the calcination temperature should be controlled because higher temperatures may lead to significant alterations in the structural properties (higher temperature lead to greater crystallinity and grain size and to lower porosity and surface area).[49,57–59]

It should be stressed that mercury porosimetry is unable to be used to measure pores that are larger than 300–400 μm. Thus, the use of this technique to analyze the Biocoral granules was infeasible.

The density values that were obtained by gas pycnometry (Table IV) are in excellent agreement with the mineral content of the corresponding samples (obtained at 600°C). In fact, the density of the anorganic samples (which exhibited mineral contents that were higher than 95%) was found to be practically identical to that of hydroxyapatite (3.16) (Bio-Oss, PepGen P-15, and calcined human bone) and to that of Aragonite (2.19) (Biocoral). As for the collagenated samples, the results show that both OsteoBiol and natural human bone resulted in a 65% mineral weight fraction [as expected from their composition (35% of collagen and water)], the density values being accordingly lower.

The specific surface areas, measured by gas adsorption (Table V), ranged from less than 1 m^2/g (Biocoral) up to 60 m^2/g (BioOss). These extremely different values are mainly due not only to the samples' surface characteristics but also to the particle size. In fact, the larger values that were exhibited by the BioOss and OsteoBiol samples are definitely associated with the fact that both samples contain cancellous bone with a rough surface. Curiously, OsteoBiol contains only 80% of cancellous bone. Its specific surface is also about 80% of that of BioOss, which is completely constituted by cancellous bone. The low values presented by PepGen P-15 (1.72 m^2/g) are not only the result of its cortical nature but also a consequence of the alterations that were induced by the heat-treatment conditions (1100°C), which created intraparticle pores that were about 10 times larger than those of BioOss or OsteoBiol (Table II). The addition of biomimetic factors as well as the least particle size of its particles certainly compensates, in terms of bone regeneration, for the reduced specific surface value. As a consequence of the coralline nature of Biocoral and also the large pores of its particles, the low surface area that was obtained was expected. This limitation will certainly be balanced by the higher dissolution rate, resulting from its chemical composition (calcium carbonate).

With the exception of Biocoral (aragonite), the FTIR spectra and XRD spectra of various materials (including human bone) were quite similar. The major difference was derived from the samples being either anorganic or collagenated. The latter possesses a lower crystallinity degree and, thus, correspond to materials that are more prone to degradation.

These differences in chemical nature and phase composition, together with those detected in the samples morphostructural properties, are expected to affect the performance of these materials after *in vivo* implantation.

CONCLUSIONS

In the present work, four commercial samples of materials currently used in dentistry were investigated. Regarding chemical composition, the tested samples can be divided into two groups: one comprising the hydroxyapatite-based materials (BioOss, PepGen P-15, and OsteoBiol) and the other constituted only by Biocoral, a calcium carbonate (aragonite) material. However, even for those with similar chemical characteristics, significant differences were detected in terms of particle size, crystallinity, porosity and pore size distribution, surface area, and mineral content.

Although these morphological characteristics greatly influence the *in vivo* behavior of the samples, they are often not taken into consideration when the samples' biological performance is evaluated. This may be responsible for the conflicting results frequently found in the literature. It is believed that the results provided for the materials investigated will be most useful to fully interpret their clinical responses.

REFERENCES

1. Finkemeier CG. Bone grafting and bone-graft substitutes. J Bone Joint Surg Am 2002;84:454–464.
2. Parikh SN. Bone graft substitutes: Past, present, future. J Postgrad Med 2002;28:142–148.
3. Torroni A. Engineered bone grafts and bone flaps for maxillofacial effects: State of the art. J Oral Maxil Surg 2009;67: 1121–1127.
4. Greenwald AS, Boden SD, Goldberg VM, Khan Y, Laurencin CT, Rosier RN. Bone-graft substitutes: Facts, fictions, and applications. J Bone Joint Surg Am 2001;83:98–103.
5. Sàndor GKB, Lindholm TC, Clokie CML. Bone regeneration of the cranio-maxillofacial and dento-alveolar skeletons in the framework of tissue engineering. In: N. Ashammakhi, P. Ferretti, editors. Topics in Tissue Engineering. 2003. Available at http://www.oulu.fi/spareparts/ebook_topics_in_t_e/abstracts/sandor_01.pdf. Oulu, Finland.
6. Block MS, Kent JN. Sinus augmentation for dental implants: The use of autogenous bone. J Oral Maxil Surg 1997;55: 1281–1286.
7. Wheeler SL. Sinus augmentation for dental implants: The use of alloplastic materials. J Oral Maxil Surg 1997;55:1287–1293.
8. Matos SM, Guerra FA, Krauser J, Marques F, Ermida J, Mariano Sanz M. Clinical evaluation of the combination of anorganic bovine-derived hydroxyapatite matrix/cell-binding peptide (P-15) in particulate and hydrogel form as a bone replacement graft material in human periodontal osseous

defects: 6-Month reentry controlled clinical study. J Periodontol 2007;78:1855–1863.
9. Ben-Nissan B. Natural bioceramics: From coral to bone and beyond. Curr Opin Solid State Mater Sci 2003;7:283–288.
10. Vehmeijer S, Bloem RM. The procurement, processing, and preservation of allograft bone. In: Delloye C, Bannister G, editors. Impaction Bone Grafting in Revision Arthroplasty. New York: Marcel Dekker; 2004. pp 23–32.
11. Urist MR. Bone formation by autoinduction. Science 1965;150:893–898.
12. Urist MR, Mikulski AJ, Nakagawa M, Yen K. A bone matrix calcification-initiator noncollagenous protein. Am J Physiol 1977;232:C115–C127.
13. Murungan R, Rao KP, Kumar TSS. Heat-deproteinated xenogeneic bone from slaughterhouse waste: Physico-chemical properties. Bull Mater Sci 2003;26:523–528.
14. Etok SE, Valsami-Jones E, Wess TJ, Hiller JC, Maxwell CA, Rogers KD, Manning DAC, White ML, Lopez-Capel E, Collins MJ, Buckley M, Penkman KEH, Woodgate SL. Structural and chemical changes of thermally treated bone apatite. J Mater Sci 2007;42:9807–9816.
15. Guillemin G, Meunier A, Dallant P, Christel P, Pouliquen J-C, Sedel L. Comparison of coral resorption and bone apposition with two natural corals of different porosities. J Biomed Mater Res 1989;23:765–779.
16. Roy DM. Linnehan SK. Hydroxyapatite formed from coral skeletal carbonate by hydrothermal exchange. Nature 1974; 247:220–222.
17. Viitala R, Franklin V, Green D, Liu C, Lloyd A, Tighe B. Towards a synthetic osteo-odonto-keratoprosthesis. Acta Biomater 2009;5:438–452.
18. Betz RR. Limitations of autograft and allograft: New synthetic solutions. Orthopedics 2002;25s:561–570.
19. Rezwan K, Chen QZ, Blaker JJ, Boccaccini AR. Biodegradable and bioactive porous polymer/inorganic composite scaffolds for bone tissue engineering. Biomaterials 2006;27:3413–3431.
20. Lutolf MP, Weber FE, Schmoekel HG, Schense JC, Kohler T, Müller R, Hubbell JA. Repair of bone defects using synthetic mimetics of collagenous extracellular matrices. Nat Biotechnol 2003;21:513–518.
21. Wang L, Nancollas GH. Calcium orthophosphates: Crystallization and dissolution. Chem Rev 2008;108:4628–4669.
22. Rabiee SM, Moztarzadeh F, Salimi-Kenari H, Solati-Hashjin M. Preparation and properties of a porous calcium phosphate bone graft substitute. Mater Sci Poland 2007;25:1019–1027.
23. LeGeros RZ. Properties of osteoconductive biomaterials: Calcium phosphates. Clin Orthop Relat Res 2002;395:81–98.
24. Daculsi G, Corre P, Malard O, Legeros R, Goyenvalle E. Performance for bone ingrowth of biphasic calcium phosphate ceramic versus bovine bone substitute. Bioceramics Jpn 2005;18:1379–1382.
25. Rumpel E, Wolf E, Kauschke E, Bienengräber V, Bayerlein T, Gedrange T, Proff P. The biodegradation of hydroxyapatite bone graft substitutes in vivo. Folia Morphol 2006;65:43–48.
26. Carvalho AL, Faria PEP, Grisi MFM, Souza SLS, Taba M, Palioto DB, Novaes AB, Fraga AF, Ozyegin LS, Oktar FN, Salata LA. Effects of granule size on the osteoconductivity of bovine and synthetic hydroxyapatite: A histologic and histometric study in dogs. J Oral Implantol 2007;33:267–276.
27. Li X, van Blitterswijk CA, Feng Q, Cui F, Watari F. The effect of calcium phosphate microstructure on bone-related cells in vitro. Biomaterials 2008;29:3306–3316.
28. Mauney JR, Jaquiéry C, Volloch V, Heberer M, Martin I, Kaplan DL. In vitro and in vivo evaluation of differentially demineralised cancellous bone scaffolds combined with human bone marrow stromal cells for tissue engineering. Biomaterials 2005;26:3173–3185.
29. Schneiders W, Reinstorf A, Pompe W, Grass R, Biewener A, Holch M, Zwipp H, Rammelt S. Effect of modification of hydroxyapatite/collagen composites with sodium citrate, phosphoserine, phosphoserine/RGD-peptide and calcium carbonate on bone remodelling. Bone 2007;40:1048–1059.
30. Qian JJ, Bhatnager RS. Enhanced cell attachment to anorganic bone mineral in the presence of a synthetic peptide related to collagen. J Biomed Mat Res 1996;31:545–554.
31. Thorwarth M, Schultze-Mosgau S, Wehrhan F, Kessler P, Srour S, Wiltfang J, Schlegel KA. Bioactivation of an anorganic bone matrix by P-15 peptide for the promotion of early bone formation. Biomaterials 2005;26:5648–5657.
32. Tadic D, Epple M. A thorough physicochemical characterisation of 14 calcium phosphate-based bone substitution materials in comparison to natural bone. Biomaterials 2004;25:987–994.
33. Schwartz Z, Boyan BD. Underlying mechanisms at the bone–biomaterial interface. J Cell Biochem 2004;56:340–347.
34. Cruz A, Pochapski M, Daher J, Silva J, Pilatti G, Santos F. Physico-chemical characterization and biocompatibility evaluation of hydroxyapatites. J Oral Sci 2006;48:219–226.
35. Annaz B, Hing KA, Kayser M, Buckland T, Di Silvio L. An ultrastructural study of cellular response to variation in porosity in phase-pure hydroxyapatite. J Microsc 2004;216:97–109.
36. Hing KA, Annaz B, Saeed S, Revell PA, Buckland T. Microporosity enhances bioactivity of synthetic bone graft substitutes. J Mater Sci: Mater Med 2005;16:467–475.
37. Geistlich Biomaterials Inc. Product information on BioOss®. 2008. Available at http://www.geistlich.ch/index.cfm?dom=2&rub=42&id=100064
38. Dentsply-Friadent. Product information on PepGen P-15®. 2008. Available at http://www.dentsply-friadent.com/en/581.htm
39. Dental & Medical Device. Product information on Osteo-Biol®. 2008. Available at http://www.dmdevice.com/tecnoss.html
40. Biocoral Inc. Product information on Biocoral®. 2008. Available at http://www.biocoral.com
41. Judas F, Teixeira L, Proença A. Coimbra University Hospitals' bone and tissue bank: Twenty-two years of experience. Transplant Proc 2005;37:2799–2801.
42. Allen T. Particle Size Measurement—Powder Sampling and Particle Size Measurement, 5th ed. Dordrecht, The Netherlands: Kluwer Academic; 1999, vol. 1.
43. Allen T. Particle Size Measurement—Surface Area and Pore Size Determination, 5th ed. Dordrecht, The Netherlands: Kluwer Academic; 1999, vol. 2.
44. Webb P, Orr C. Analytical Methods in Fine Particle Technology. Norcross, GA: Micromeritics Instrument Corporation; 1997.
45. Mineralogy Database. General information on hydroxyapatite. 2008. Available at http://webmineral.com/data/Hydroxylapatite.shtml
46. Mineralogy Database. General information on aragonite. 2008. Available at http://webmineral.com/data/Aragonite.shtml
47. Mkukuma LD, Skakle JMS, Gibson IR, Imrie CT, Aspden RM, Hukins DWL. Effect of the proportion of organic material in bone on thermal decomposition of bone mineral: An investigation of a variety of bones from different species using thermogravimetric analysis coupled to mass spectrometry, high temperature x-ray diffraction and Fourier transform infrared spectroscopy. Calcif Tissue Int 2004;75:321–328.
48. Thamaraiselvi TV, Prabakaran K, Rajeswari S. Synthesis of hydroxyapatite that mimic bone minerology. Trends Biomater Artif Organs 2006;19:81–83.

49. Ooi CY, Hamdi M, Ramesh S. Properties of hydroxyapatite produced by annealing of bovine bone. Ceramics Int 2007;33: 1171–1177.
50. Peters F, Schwarz K, Epple M. The structure of bone studied with synchrotron X-ray diffraction, X-ray absorption spectroscopy and thermal analysis. Thermochim Acta 2000;361:131–138.
51. Barreiros FM, Ferreira PJ, Figueiredo MM. Calculating shape factors from particle sizing data. Part Part Syst Char 1996;13: 368–373.
52. Moreira A, Pastoreli MT, Damasceno LHF, Defino HLA. Influence of dimensions of hydroxyapatite granules upon bone integration: An experimental study. Acta Ortop Bras 2003;11: 240–250.
53. Sun JS, Liu HC, Chang WHS, Li J, Lin FH, Tai HC. Influence of hydroxyapatite particle size on bone cell activities: An in vitro study. J Biomed Mater Res 1998;39:390–397.
54. Karageorgiou V, Kaplan D. Porosity of 3D biomaterial scaffols and osteogenesis. Biomaterials 2005;26:5474–5491.
55. Murungan R, Ramakrishna S, Rao KP. Nanoporous hydroxycarbonate apatite scaffold made of natural bone. Mater Lett 2006;60:2844–2847.
56. Makoto M, Ito EM, Takahata EM, Kadoya KE, Irie EK, Minami EA. Effect of hydroxyapatite porous characteristics on healing outcomes in rabbit posterolateral spinal fusion model. Eur Spine J 2007;16:2215–2224.
57. Haberko K, Bucko MM, Brzezinska-Miecznik J, Haberko M, Mozgawa W, Panz T, Pyda A, Zarebski J. Natural hydroxyapatite—Its behaviour during heat treatment. J Eur Ceram Soc 2006;26:537–542.
58. Melville A, Lorenzo LMR, Forshyte JS. Effects of calcination temperature on the drug delivery behaviour of Ibuprofen from hydroxyapatite powders. J Mater Sci Mater Med 2008;19: 1187–1195.
59. Hiller JC, Thompson TJU, Evison MP, Chamberlain AT, Wess TJ. Bone mineral change during experimental heating: An X-ray scattering investigation. Biomaterials 2003;24: 5091–5097.